Crystal and magnetic structures of the colossal magnetoresistance manganates $Sr_{2-x}Nd_{1+x}Mn_2O_7$ ($x=0.0$, 0.1)

P. D. Battle,* M. A. Green, N. S. Laskey, and J. E. Millburn
Inorganic Chemistry Laboratory, University of Oxford, South Parks Road, Oxford OX1 3QR, United Kingdom

P. G. Radaelli
Institut Laue-Langevin, P.O. Box 156, 38042 Grenoble Cedex 9, France

M. J. Rosseinsky,* S. P. Sullivan, and J. F. Vente
Inorganic Chemistry Laboratory, University of Oxford, South Parks Road, Oxford OX1 3QR, United Kingdom
(Received 15 July 1996)

Neutron powder diffraction techniques have been used to refine the crystal and magnetic structures of the Ruddlesden Popper (RP) compounds $Sr_{2-x}Nd_{1+x}Mn_2O_7$ ($x=0.0$, 0.1), which show colossal magnetoresistance below 100 K. Samples of both compositions have been shown to be biphasic, although in each case both phases are of the RP type and have very similar structural parameters. Only one phase in each sample shows long range magnetic order. For $x=0.0$, the Mn cations and the Nd cations in the rocksalt layers of the structure are antiferromagnetically ordered in a noncollinear magnetic structure below 28 K; the Nd cations within the perovskite blocks do not show long range magnetic order. In the temperature range $28 \leqslant T/K \leqslant 137$, only the Mn cations are ordered. The decoupling of the Nd cations is accompanied by a rotation of the Mn moments from a direction close ($\phi=27°$) to the z axis into the xy plane. A similar temperature dependence is seen in the case $x=0.1$, although the ordered components of the cation moments are much reduced and the low temperature phase has a collinear magnetic structure with the moments aligned along z. The magnetotransport properties of these samples are discussed in the light of their crystal and magnetic structures. [S0163-1829(96)07246-3]

INTRODUCTION

The observation of colossal magnetoresistance (CMR) in the pseudocubic perovskites $Ln_{1-x}A_xMnO_3$ (A=Ca, Ba, Sr, Pb, Bi) has attracted considerable attention.[1–5] Similar behavior has recently been observed in the pyrochlore $Tl_2Mn_2O_7$ (Ref. 6) and in the Ruddlesden-Popper (RP) phase $Sr_{1.8}La_{1.2}Mn_2O_7$.[7] All these manganates, which have an insulating, high-temperature paramagnetic phase and a metallic, low-temperature ferromagnetic phase, show CMR in a relatively small temperature range around the Curie temperature, indicating a strong relationship between electrical resistivity and spin alignment. The observed magnetoresistance arises because the additional spin alignment caused by the external field effectively moves the metal-insulator transition to $T \geqslant T_c$. Recently, our attention has been focused on a group of compounds that do not show a transition to a fully ordered ferromagnetic state but which do show a large magnetoresistance effect.[8,9] We have observed a magnetoresistance ratio, $(\rho_B-\rho_0)/\rho_B$, of -4×10^4% at 4.2 K and 14 T for $Sr_2NdMn_2O_7$, and of -3×10^5% at 40 K and 14 T for $Sr_{1.9}Nd_{1.1}Mn_2O_7$. These compounds are isostructural with the $n=2$ member of the series of Ruddlesden-Popper (RP) phases $A_{n+1}Mn_nO_{3n+1}$.[10,11] The RP phases can be thought to consist of perovskitelike blocks n octahedra thick, separated by a rock-salt-type $(Sr,Ln)_2O_2$ layer.[12] The perovskite structure corresponds to $n=\infty$, and the K_2NiF_4 structure to $n=1$. The double layer ($n=2$) compounds can be prepared for a wide variety of elements, and the structure of such a compound is drawn in Fig. 1. Among the structural consequences of moving from perovskite to $n=2$ RP are the introduction of a two-dimensional character and a reduction from 6 to 5 in the number of nearest-neighbor Mn cations around each transition-metal site. This is expected to produce an anisotropic reduction in the width of the energy bands derived (largely) from the Mn 3d orbitals, and hence to modify the electrical and magnetic properties. In the case of $Sr_{2-x}La_{1+x}Mn_2O_7$, a metal-insulator transition can be observed at ~130 K.[7,8] This transition is accompanied by the appearance of a spontaneous magnetization. In contrast, $Sr_2NdMn_2O_7$ is semiconducting throughout the temperature range $4 \leqslant T/K \leqslant 300$, and magnetic susceptibility measurements indicate the existence at low temperatures of a complex behavior in which magnetic frustration seems to play an important role. $Sr_{1.9}Nd_{1.1}Mn_2O_7$ is also semiconducting below 300 K, but the temperature dependence of the sample magnetization, although again complex, shows significant differences from that of $Sr_2NdMn_2O_7$. It is particularly interesting that both Nd-containing compounds show magnetoresistance ($>10^4$%) over a wide temperature range ($4 \leqslant T/K \leqslant 100$), but neither shows a spontaneous magnetization. The observation of CMR in the absence of ferromagnetism distinguishes these compounds from all other CMR materials. In this paper we describe the crystal chemistry and magnetic structures of RP $Sr_{2-x}Nd_{1+x}Mn_2O_7$ ($x=0.0$, 0.1) as determined from neutron diffraction data.

EXPERIMENT

The preparation of $Sr_{2-x}Nd_{1+x}Mn_2O_7$ ($x=0.0$, 0.1) and their preliminary structural characterization by x-ray powder diffraction have been described elsewhere.[8,9,13] Neutron dif-

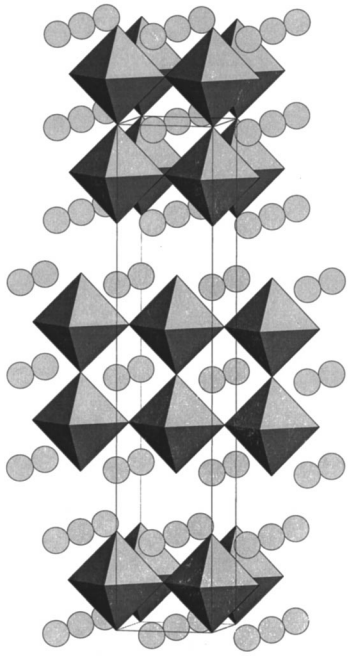

FIG. 1. The $n=2$ Ruddlesden-Popper crystal structure of $Sr_{2-x}Nd_{1+x}Mn_2O_7$. MnO_6 octahedra are shaded and the Sr/Nd sites are shown as circles.

fraction patterns were collected in the temperature range $1.6 \leqslant T/K \leqslant 300$ on the powder diffractometers D1b (mean wavelength 2.520 Å, $5 \leqslant 2\theta/° \leqslant 85$) and D2b (mean wavelengths 1.59412 Å and 2.3979 Å, $5 \leqslant 2\theta/° \leqslant 150$, $\Delta 2\theta = 0.05°$) at the Institut Laue Langevin, Grenoble, France.[14,15] The former is a low resolution instrument which is best used to collect diffraction patterns rapidly as a function of, for example, temperature. The latter is a higher resolution instrument producing data which facilitate detailed structure analysis. Data were collected on samples contained in cylindrical vanadium cans with diameters of between 5 and 10 mm. All diffraction patterns were, analyzed with the Rietveld technique[16] using the program package GSAS.[17] The following neutron scattering lengths were used: $b_{Sr}=0.702$, $b_{La}=0.827$, $b_{Nd}=0.769$, $b_{Mn}=-0.373$, and $b_O=0.5805\times10^{-14}$ m. The free ion form factors of Mn^{3+} (Ref. 18) and Nd^{3+} (Ref. 19) were used to describe the angular dependence of the magnetic scattering amplitude. The background was fitted with a twelfth order shifted Chebychev polynomial and the shape of the Bragg peaks was described by a four term pseudo-Voigt function.

RESULTS

A. $Sr_2NdMn_2O_7$

The diffraction pattern of $Sr_2NdMn_2O_7$ collected on D2b ($\lambda \sim 1.6$ Å) at room temperature could be indexed in an apparently satisfactory way on the basis of an $n=2$ RP structure with space group $I4/mmm$; the crystallography of this structure is summarized in Table I. Attempts to refine the structure using this simple model resulted in a reasonable level of agreement between the observed and calculated diffraction profiles ($R_{wpr}=7.3\%$). However, we were unable to achieve a satisfactory level of agreement when the same model (which used isotropic temperature factors for the crystallographically different atoms) was used to account for the data collected at 1.7 K ($R_{wp}=9.89\%$). There was a considerable mismatch between calculated and observed peak positions at $2\theta > 80°$ in the low temperature data set. The value of R_{wp} fell to 8.49% when anisotropic temperature factors, preferred orientation along [001], and anisotropic peak broadening (for the reflections $\{hkl\}$, $l \neq 0$) were included in the model, but the fit was still not considered satisfactory. We were able to model our data in a more convincing way by

TABLE I. Generalized crystallography for the $n=2$ Ruddlesden-Popper structure, space group $I4/mmm$.

Atoms	Site	Coordinates
Sr/Ln(1)	2*b*	0 0 1/2
Sr/Ln(2)	4*e*	0 0 *z*; $z \sim 0.7$
Mn	4*e*	0 0 *z*; $z \sim 0.1$
O(1)	2*a*	0 0 0
O(2)	4*e*	0 0 *z*; $z \sim 0.2$
O(3)	8*g*	0 1/2 *z*; $z \sim 0.1$

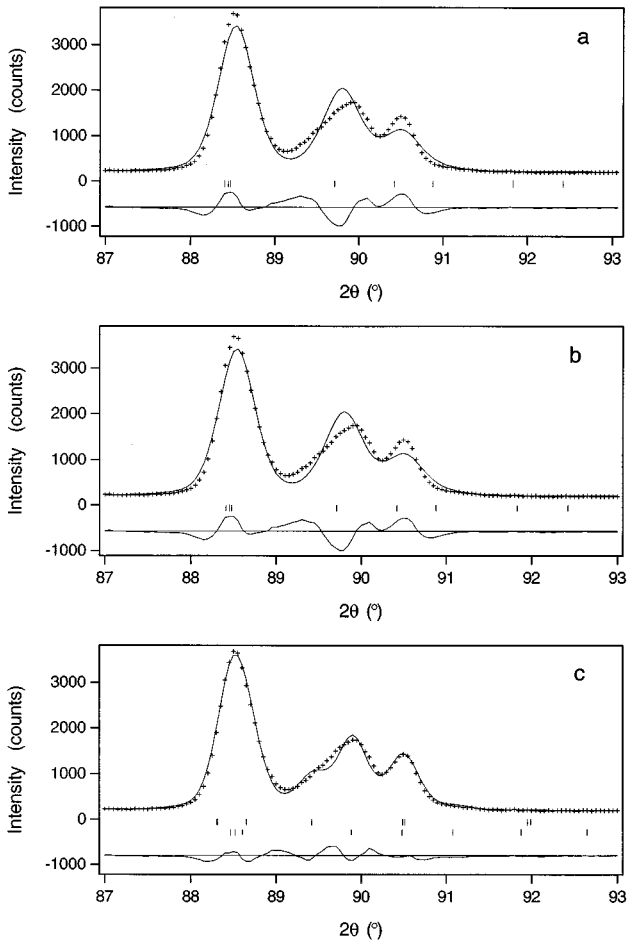

FIG. 2. Neutron diffraction profile of $Sr_2NdMn_2O_7$ modeled as (a) single phase, symmetric peak profile, (b) single phase, anisotropic peak profile, and (c) two phases, isotropic peak profile.

TABLE II. Crystallographic data for $Sr_2NdMn_2O_7$ at 290 K.

	Phase 1	Phase 2
a (Å)	3.84905(6)	3.8451(1)
c (Å)	19.9599(7)	20.022(1)
V (Å^3)	295.711(9)	296.02(2)
Fraction (%)	65(2)	35(2)
U_{iso} (Sr/Nd1) (Å^2)	0.003(1)	0.002(2)
z (Sr/Nd2)	0.6833(1)	0.6814(3)
U_{iso} (Sr/Nd2) (Å^2)	0.002(1)	0.006(2)
z (Mn)	0.0966(3)	0.0953(7)
U_{iso} (Mn) (Å^2)	0.001(1)	0.005(3)
U_{iso} (O1) (Å^2)	0.015(2)	0.014(3)
z (O_2)	0.1946(3)	0.1984(5)
U_{iso} (O2) (Å^2)	0.009(1)	0.026(4)
z (O3)	0.0953(2)	0.0968(4)
U_{iso} (O3) (Å^2)	0.0079(7)	0.008(1)
R_{wp}, R_p (%)	6.12	4.40
χ^2_{red} DWd	5.54	0.35

assuming that the sample consisted of two essentially isostructural phases with slightly different unit cell parameters. The compositions of the two phases were too similar to be distinguished, particularly in view of the similarity between the scattering lengths of Sr and Nd. Analysis of the data collected at 1.7 K using only an overall, isotropic temperature factor for each phase resulted in relative phase fractions 65:35 (R_{wp}=7.37%); four parameters, common to both phases, were used to model a symmetrical peak shape and no allowance was made for preferred orientation. The improvement produced by the use of this two phase model (Fig. 2) was enough to convince us of its validity, and we therefore reanalyzed our room temperature data using this approach, but with individual isotropic temperature factors for each atom. The phase fractions refined to the same values as in the analysis of the low temperature data, thus justifying the use of the model. The atomic coordinates derived from a two-phase refinement (R_{wp}=6.12%) of the room temperature structure of $Sr_2NdMn_2O_7$ and the derived bond distances and angles are given in Tables II and III. The Sr and Nd cations were assumed to be disordered over two crystallographic

TABLE III. Bond lengths (Å) and selected bond angles (°) in $Sr_2NdMn_2O_7$ at 290 K.

		Phase 1	Phase 2
Mn-O(1)	(1×)	1.928(7)	1.91(1)
Mn-O(2)	(1×)	1.956(9)	2.06(1)
Mn-O(3)	(4×)	1.924(8)	1.92(1)
Mn-Mn ($z,-z$)		3.85(1)	3.82(1)
Sr/Nd(1)-O(1)	(4×)	2.721(4)	2.719(4)
Sr/Nd(1)-O(3)	(8×)	2.707(5)	2.731(5)
Sr/Nd(2)-O(2)	(1×)	2.436(6)	2.40(1)
Sr/Nd(2)-O(2)	(4×)	2.731(6)	2.74(1)
Sr/Nd(2)-O(3)	(4×)	2.606(4)	2.562(7)
O(1)-Mn-O(3)		89.3(2)	90.9(4)
O(3)-Mn-O(3)		178.5(5)	178.1(9)

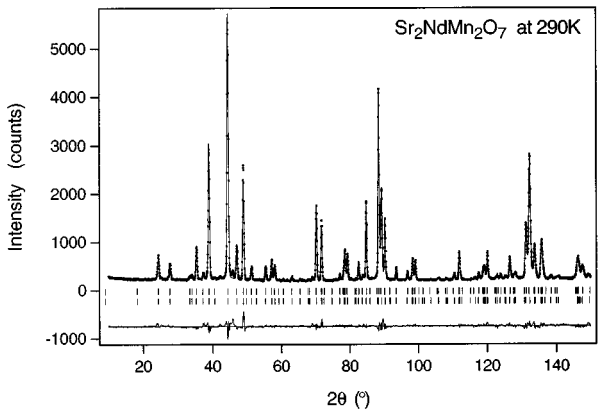

FIG. 3. Observed, calculated, and difference neutron powder diffraction patterns for $Sr_2NdMn_2O_7$ at 290 K (λ~1.6 Å). Reflection positions are marked for both phase 1 (lower) and phase 2 (upper).

sites. Figure 3 shows the final observed and calculated diffraction patterns. The structural parameters and bond lengths derived from the experiments performed at 1.7 K are presented in Tables IV and V, and the diffraction profiles are plotted in Fig. 4. The cation environments in $Sr_2NdMn_2O_7$ at 290 K are drawn in Fig. 5. The consequences of the constraints imposed on the peak profiles and the temperature factors in these refinements are discussed below.

Arriving at the interpretation of the diffraction patterns described above was made more difficult by the presence of additional, magnetic Bragg peaks in the low temperature data sets. The development of the neutron diffraction pattern of $Sr_2NdMn_2O_7$ as a function of the temperature is shown at low resolution in Fig. 6, using data collected on D1b at temperature intervals of 4 K. Magnetic Bragg peaks first appear at 137±2 K, and there is a change in their relative intensities at 28±2 K. The additional peaks could all be indexed using the chemical unit cell, but the presence of $\{00l\}$ peaks with $l=2n+1$ indicates that the magnetic structure is not body centered. It was concluded, following an initial analysis of

TABLE IV. Crystallographic and magnetic data for $Sr_2NdMn_2O_7$ at 1.7 K.

	Phase 1	Phase 2
a (Å)	3.85062(8)	3.8404(2)
c (Å)	19.8367 (7)	19.947(1)
V (Å^3)	294.12(1)	294.2(2)
Fraction (%)	65(3)	35(3)
z (Sr/Nd2)	0.6826(2)	0.6819(3)
z (Mn)	0.0959(3)	0.0950(7)
z (O2)	0.1965(2)	0.1944(4)
z (O3)	0.0948(2)	0.0980(3)
U_{iso} (Å^2)	0.0009(4)	0.0067(8)
μ_{Mn} (μ_B)	3.08(4)	
ϕ_{Mn} (°)	27.6(12)	
μ_{Nd} (μ_B)	2.02(10)	
R_{wp}, R_p (%)	7.37	5.55
χ^2_{red}, DWd	9.65	0.221

TABLE V. Bond lengths (Å) and selected bond angles (°) in $Sr_2NdMn_2O_7$ at 1.7 K.

		Phase 1	Phase 2
Mn-O(1)	(1×)	1.902(7)	1.90(1)
Mn-O(2)	(1×)	1.996(8)	1.98(2)
Mn-O(3)	(4×)	1.925(8)	1.92(2)
Mn-Mn $(z,-z)$		3.80(1)	3.78(1)
Sr/Nd(1)-O(1)	(4×)	2.722(6)	2.72(1)
Sr/Nd(1)-O(3)	(8×)	2.691(6)	2.74(1)
Sr/Nd(2)-O(2)	(1×)	2.398(5)	2.46(1)
Sr/Nd(2)-O(2)	(4×)	2.737(5)	2.73(1)
Sr/Nd(2)-O(3)	(4×)	2.597(6)	2.546(7)
O(1)-Mn-O(3)		89.3(2)	91.8(5)
O(3)-Mn-O(3)		178.7(4)	176.4(1)

D2b data in which the unit cell parameters of the magnetic structure were not tied to either structural phase, that only the majority phase orders magnetically. The appropriate constraints were then applied in subsequent refinements; we shall return to this point below. The complex magnetic structure is shown in Fig. 7. The lanthanide elements in the disordered sheets of Sr(1) and Nd(1) which lie within the octahedral double layers (at $z=0$, 1/2) do not contribute to the long range magnetic order. The magnetic moments of the Nd(2) cations in the rocksalt layer align along the crystallographic z axis to form ferromagnetic sheets which lie perpendicular to that axis; the Nd spins at the top and bottom of each double layer of MnO_6 octahedra align antiparallel. Similarly, the two sheets of Mn cations within each octahedral double layer align in an antiferromagnetic manner, albeit in a direction which makes an angle $\phi\sim27°$ with z; the z component of the Mn moment is parallel to that of the closest Nd(2) cation. Each double layer can therefore be thought of as an antiferromagnetic unit. A translation of (1/2,1/2,1/2), that is a move to an identical atom in the next double layer, results in a reversal of the spin direction, and the magnetic structure is thus antibody centered. At room temperature the distance between the Mn atoms at $(00z)$ and $(00\text{-}z)$ in the majority phase is very similar to the Mn-Mn distance in the xy plane (equal to the unit cell parameter a), but at 1.7 K the former (3.80 Å) is much less than the latter (3.85 Å). This anisotropic distortion, which has the effect of shortening the antiferromagnetic superexchange pathways whilst lengthening those between ferromagnetically aligned cations, is not observed in the minority phase. It is thus likely to be an exchange striction effect[20] rather than the result of anisotropic thermal contraction, which would be expected to affect two such similar phases to an approximately equal extent. The observation of this effect in only one of the two components thus provides strong evidence for our assumption that there is only one magnetically ordered phase. It is interesting to take another view of the structure and to think of it as consisting of magnetic blocks perpendicular to z which are four atom-layers [Mn+Nd+Nd+Mn] thick. These magnetic blocks are separated from each other by the nonmagnetic Sr/Nd layers. Each block has a net magnetization which lies close to z, and the magnetizations of neighboring blocks are antiparallel. We shall use this second description of the magnetic structure in our discussion below.

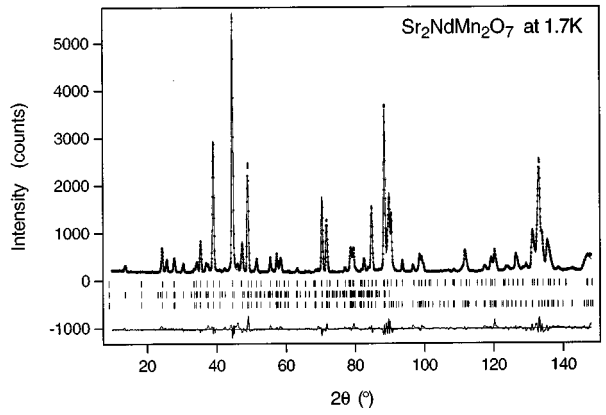

FIG. 4. Observed, calculated, and difference neutron powder diffraction patterns for $Sr_2NdMn_2O_7$ at 1.7 K ($\lambda\sim1.6$ Å). Reflection positions are marked for the phase 1 (lower) and phase 2 (upper) as well as for the allowed magnetic reflections (central).

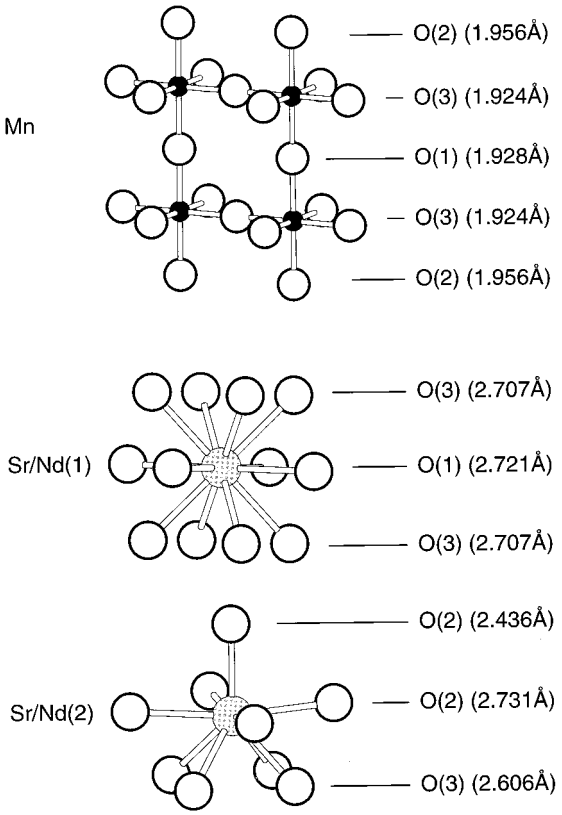

FIG. 5. The cation environments in $Sr_2NdMn_2O_7$ at 290 K.

The evolution of the magnetic structure of $Sr_2NdMn_2O_7$ with temperature was quantified by analyzing the individual diffraction patterns which make up Fig. 6. The atomic coordinates were held constant during the course of these refinements which were concerned primarily with the magnitude and direction of the ordered atomic magnetic moments. Their outcome is summarized in Fig. 8. In the temperature range $1.7\leqslant T/K\leqslant35$, the magnitude of the Mn moment remains essentially constant, whereas the ordered component of the Nd moment decreases, becoming insignificant above 30 K.

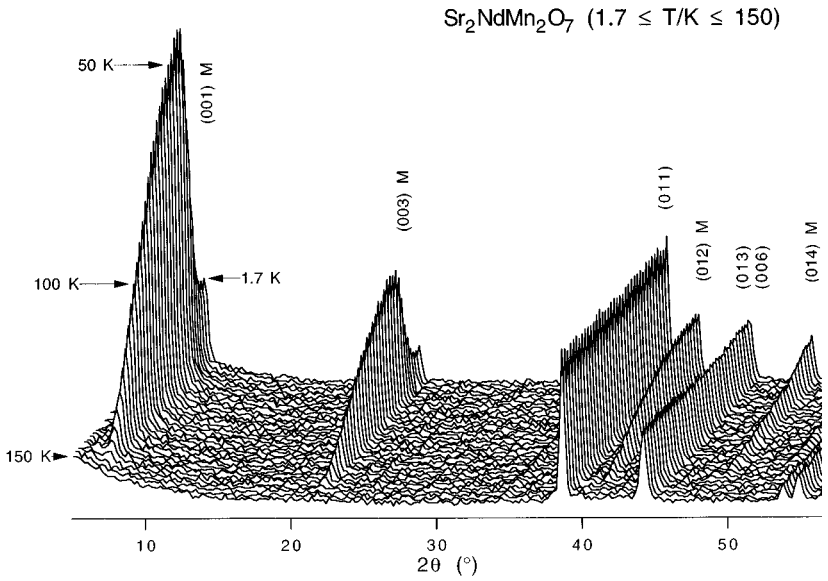

FIG. 6. The development of the neutron diffraction pattern for $Sr_2NdMn_2O_7$ as a function of the temperature in the angular range $5 \leqslant 2\theta/° \leqslant 55$ ($\lambda \sim 2.5$ Å). The Bragg reflections are indexed and the magnetic peaks are marked.

As the Nd moment diminishes, the Mn moments rotate until, at ~30 K, they lie perpendicular to the z axis ($\phi = 90°$). The magnitude of the latter moments does decrease at higher temperatures, with the magnetic Bragg peaks being lost in the experimental noise above ~140 K. The antiferromagnetic structure in the temperature range $30 \leqslant T/K \leqslant 140$ is thus that drawn in Fig. 9. It should be noted that we have chosen to work with a magnetic model in which the spins on each sublattice (Mn and Nd) are collinear, thereby reducing the symmetry of the magnetic structure to orthorhombic. It is, however, impossible to determine the spin direction in the xy plane when only powder diffraction data are available.

The values of the magnetic moments derived in the data analysis described above depend on the validity of the conclusion that only the majority phase shows long range magnetic ordering. In order to obtain further evidence for this we determined the unit cell parameters of the two coexisting phases as a function of temperature by a full profile analysis of high resolution data collected on D2b. The results plotted in Fig. 10 show that the unit cell parameters and the cell volume of the minority phase decrease smoothly with tem-

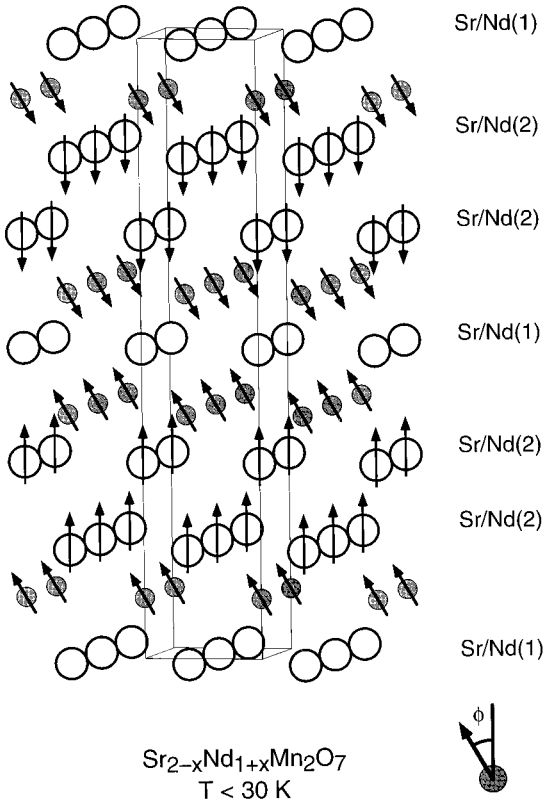

FIG. 7. The magnetic structure of $Sr_2NdMn_2O_7$ at 1.7 K. Mn atoms are shaded and the Nd atoms are shown as unshaded circles. Arrows indicate the directions of the magnetic moments.

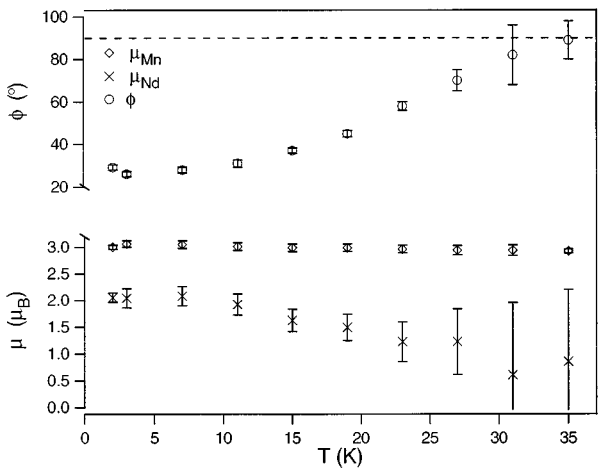

FIG. 8. The average ordered magnetic moments of Mn (diamonds) and of Nd (crosses) and the direction of the moment of Mn with respect to the z axis (circles) as a function of temperature between 1.7 and 35 K.

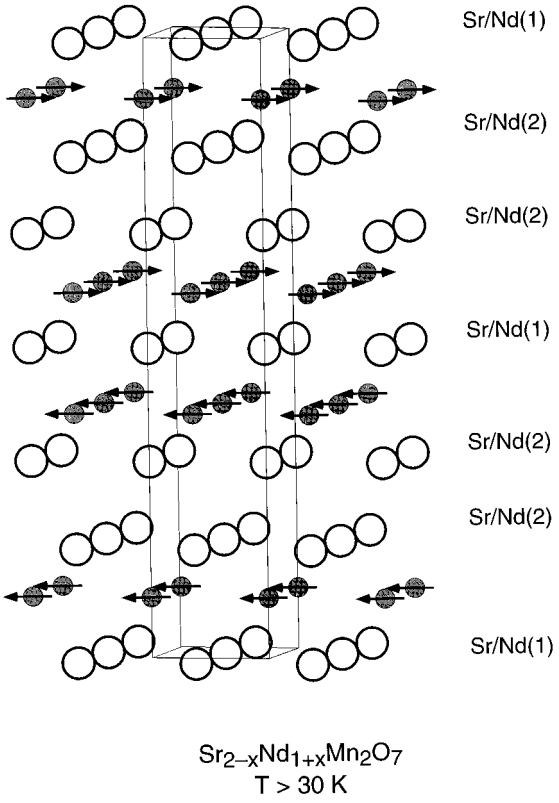

FIG. 9. The magnetic structure of $Sr_2NdMn_2O_7$ in the temperature range $30 \leq T/K \leq 140$. Mn sites are shaded and the Nd atoms are shown as unshaded circles. Arrows indicate the direction of the magnetic moments.

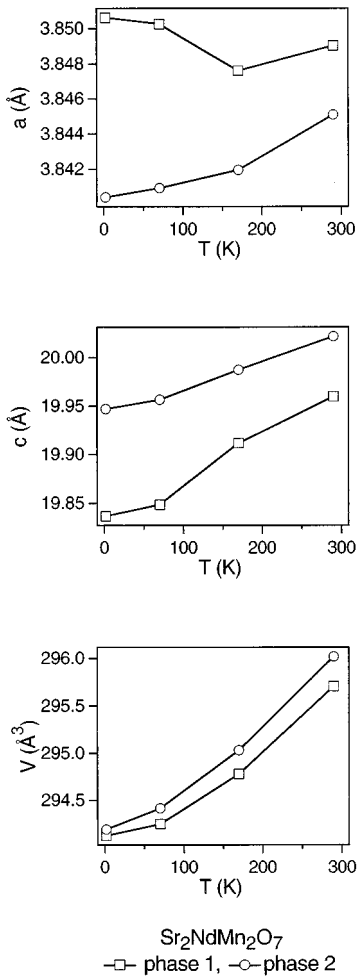

FIG. 10. Unit cell parameters *a* (a), *c* (b), and the unit cell volume (c) of $Sr_2NdMn_2O_7$ as a function of the temperature. Phase 1 is the majority phase.

perature whereas the *a* parameter of the majority phase increases on cooling below 170 K even though the cell volume continues to fall. This phase-specific change in gradient, occurring in the temperature range where magnetic scattering is first observed (Fig. 6), provides convincing evidence that the magnetic phase transition is associated only with the majority phase. It is certainly not associated solely with the minority phase because such an assumption leads to unphysical values $[4.07(5)\mu_B]$ for the ordered magnetic moment on the Mn cations. The relative phase fraction was allowed to vary during these refinements but it did not deviate from the value determined at 1.7 K and room temperature.

B. $Sr_{1.9}Nd_{1.1}Mn_2O_7$

Profile analysis of data collected from $Sr_{1.9}Nd_{1.1}Mn_2O_7$ on D2b at 1.7 K indicated the presence of two $n=2$ RP phases in the ratio 46:54. At high temperatures the two sets of unit cell parameters were too close in value to permit a free refinement of the relative phase fraction, which was therefore constrained to the value determined at 1.7 K. The 290 K structural parameters and bond lengths are listed in Tables VI and VII and the observed and calculated diffraction profiles are plotted in Fig. 11. The data collected at 1.7 K showed clear evidence of magnetic ordering, but the observed magnetic scattering was markedly diminished compared to that from $Sr_2NdMn_2O_7$. In particular, the $\{00l\}$ reflections with $l=2n+1$ were absent. The data were accounted for in a satisfactory way using the same basic magnetic model as in the case of $Sr_2NdMn_2O_7$, but with the spins on both the Mn and Nd sublattices aligned along z; the xy component refined to zero. This is consistent with the absence of $\{00l\}$ magnetic reflections. The refined structural and magnetic parameters are listed in Table VIII and the bond lengths are presented in Table IX. The observed and calculated diffraction profiles are plotted in Fig. 12.

D2b was used to collect further diffraction data sets on $Sr_{1.9}Nd_{1.1}Mn_2O_7$ at selected temperatures in the range $1.7 \leq T/K \leq 160$. No structural phase transitions were observed but, as in the case of $Sr_2NdMn_2O_7$, the Nd cations in the rocksalt layers ceased to contribute to the magnetic Bragg scattering at a relatively low temperature and the magnetic moments of the Mn cations rotated to lie in the ab plane. As a result of the nature of our experiment we cannot identify the transition temperature precisely, but it lies below 30 K. The average ordered moment per Mn cation is plotted as a function of temperature in Fig. 13. No magnetic peaks were visible in data sets collected at $T>120$ K. By analogy with $Sr_2NdMn_2O_7$, the analysis of these data was carried out assuming that only one of the two phases present shows long range magnetic order. The temperature dependence of the unit cell parameters drawn in Fig. 14 indicated that it was

TABLE VI. Crystallographic data for $Sr_{1.9}Nd_{1.1}Mn_2O_7$ at 290 K.

	Phase 1	Phase 2
a (Å)	3.84567(6)	3.84219(7)
c (Å)	20.0266(6)	20.0831(7)
V (Å^3)	296.17(1)	296.48(1)
Fraction (%)	46[a]	54[a]
U_{iso} (Sr/Nd1) (Å^2)	0.000(1)	0.003(1)
z (Sr/Nd2) (Å^2)	0.6834(2)	0.6820(2)
U_{iso} (Sr/Nd2) (Å^2)	0.0015(9)	0.0042(9)
z (Mn)	0.0965(4)	0.0969(5)
U_{iso} (Mn) (Å^2)	0.000(1)	0.010(2)
U_{iso} (O1) (Å^2)	0.015(2)	0.018(2)
z (O2)	0.1961(3)	0.1978(3)
U_{iso} (O2) (Å^2)	0.018(2)	0.019(2)
z (O3)	0.0954(2)	0.0970(2)
U_{iso} (O3) (Å^2)	0.0077(7)	0.0102(7)
R_{wp}, R_p (%)	6.32	4.43
χ^2_{red}, DWd	5.03	0.38

[a]Constrained at the value obtained from the refinement at 1.7 K.

again the phase with the lower c/a ratio, in this case the minority component (phase 1).

DISCUSSION

The structural chemistry of this system is clearly complex, and further experimentation is needed in order to establish the equilibrium phase diagram. [Prolonged heating of our samples at 1300 °C for 17 days resulted in the formation of a perovskite ($n=\infty$) phase, thus indicating that we are working with metastable compositions.] Before discussing our results in depth, we should focus attention on the assumptions made during the course of our Rietveld analyses. The use of only an overall isotropic temperature factor for each phase in the refinement of the low temperature structure of $Sr_2NdMn_2O_7$ could be considered inadequate, particularly when the refined values differ markedly despite the similarities between the two phases. Refinements using different temperature factors for each atom, but with the corresponding atoms in the two phases constrained to have the same value, resulted in parameters which were significantly negative, and therefore unphysical. We have consequently chosen to report the former model, despite the latter having a lower R factor (6.32%). Similarly, we were able to obtain an improved fit by allowing the parameter (L_y) which defines the Lorentzian component of the peak shape to vary between phases, but the resultant sevenfold difference in values was felt to be unacceptably large. Furthermore, the relaxation of the constraints on this parameter caused large correlations (up to 98%) and variations in others, particularly the relative phase fractions, and consequently, the magnitudes of the ordered magnetic moments. Hence these parameters cannot be considered to be well determined by our analysis. However, the basic magnetic structure, the unit cell parameters, and the assumption that only one magnetic phase is present proved to be robust in all our refinements. The latter relies only on the determination of peak positions, and not on the deconvolution of intensities. The model dependence of the bond lengths was also minimal. Thus we conclude that uncertainties in excess of the statistical fitting errors are associated

TABLE VII. Bond lengths (Å) and selected bond angles (°) in $Sr_{1.9}Nd_{1.1}Mn_2O_7$ at 290 K.

		Phase 1	Phase 2
Mn-O(1)	(1×)	1.93(1)	1.94(1)
Mn-O(2)	(1×)	1.99(1)	2.02(1)
Mn-O(3)	(4×)	1.92(1)	1.92(1)
Mn-Mn ($z,-z$)		3.86(1)	3.89(1)
Sr/Nd(1)-O(1)	(4×)	2.719(5)	2.716(5)
Sr/Nd(1)-O(3)	(8×)	2.711(4)	2.737(4)
Sr/Nd(2)-O(2)	(1×)	2.411(7)	2.414(7)
Sr/Nd(2)-O(2)	(4×)	2.731(7)	2.735(7)
Sr/Nd(2)-O(3)	(4×)	2.609(5)	2.569(5)
O(1)-Mn-O(3)		89.3(3)	90.1(3)
O(3)-Mn-O(3)		178.7(6)	179.8(6)

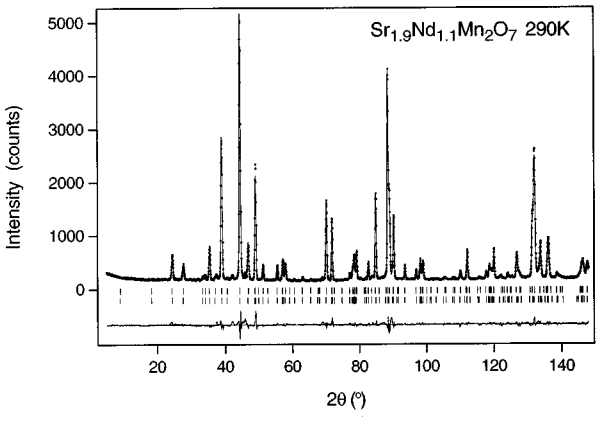

FIG. 11. Observed, calculated, and difference neutron powder diffraction patterns for $Sr_{1.9}Nd_{1.1}Mn_2O_7$ at 290 K ($\lambda\sim1.6$ Å). Reflection positions are marked for both the majority and minority phases as in Fig. 3.

TABLE VIII. Crystallographic and magnetic data for $Sr_{1.9}Nd_{1.1}Mn_2O_7$ at 1.7 K.

	Phase 1	Phase 2
a (Å)	3.8448(1)	3.8376(1)
c (Å)	19.9313(9)	20.0148(9)
V (Å^3)	294.64(1)	294.76(2)
Fraction (%)	46(3)	54(3)
z (Sr/Nd2)	0.6824(2)	0.6818(2)
z (Mn)	0.0953(5)	0.0956(5)
z (O2)	0.1960(3)	0.1981(3)
z (O3)	0.0960(2)	0.0966(3)
U_{iso} (Å^2)	0.0027(7)	0.0054(6)
μ_{Mn} (μ_B)	2.16(7)	
μ_{Nd} (μ_B)	1.62(14)	
R_{wp}, R_p (%)	7.65	5.50
χ^2_{red}, DWd	9.19	0.231

TABLE IX. Bond lengths (Å) and selected bond angles (°) in $Sr_{1.9}Nd_{1.1}Mn_2O_7$ at 1.7 K.

		Phase 1	Phase 2
Mn-O(1)	(1×)	1.90(1)	1.91(1)
Mn-O(2)	(1×)	2.00(1)	2.05(1)
Mn-O(3)	(4×)	1.922(6)	1.918(8)
Mn-Mn $(z,-z)$		3.79(1)	3.83(1)
Sr/Nd(1)-O(1)	(4×)	2.718(7)	2.713(7)
Sr/Nd(1)-O(3)	(8×)	2.713(4)	2.724(4)
Sr/Nd(2)-O(2)	(1×)	2.423(8)	2.403(6)
Sr/Nd(2)-O(2)	(4×)	2.732(7)	2.733(8)
Sr/Nd(2)-O(3)	(4×)	2.580(6)	2.567(5)
O(1)-Mn-O(3)		90.4(3)	90.6(3)
O(3)-Mn-O(3)		179.1(7)	178.8(6)

with some of the parameters in any model used to reproduce the experimental data on this complex system, but that the fundamental features of the model are well established.

With these limitations in mind, consideration of the results (Tables II and III) obtained from the sample of overall composition $Sr_2NdMn_2O_7$ shows that Mn-O(2), a bond directed out of the double octahedral layer in the z direction, shows the most striking change in length between phases 1 and 2. This increase, which is apparent to a lesser extent in $Sr_{1.9}Nd_{1.1}Mn_2O_7$ (Table VII), is associated with the relatively large unit cell parameter c of phase 2. However, the mean Mn-O bond length does not differ significantly from one phase to the other, nor from one composition to the other. In both samples the Sr/Nd(1) site is larger than the Sr/Nd(2) site, as is to be expected in view of the larger coordination number. More interestingly, in both cases the Sr/Nd(1) site (perovskite layer) is significantly larger for phase 2 than for phase 1, whereas the Sr/Nd(2) site (rocksalt layer) is, in both cases, larger for phase 1. This suggests that the cation distribution over the two sites is different in the two phases, a relatively large size being representative of an increased Sr concentration on that site. However, the similarity in volume of the two phases suggests that the overall Sr/Nd ratio is the same in both. This is a very significant observation because it implies that we are not simply dealing with a sample of poor bulk homogeneity, but rather with a system in which subtle crystal-chemical effects are operating at a local level. This behavior derives from the near-identical structural requirements of Sr^{2+} and Nd^{3+}, and leads to the strikingly different properties of two phases in a homogeneous sample. The relatively large standard deviations associated with the Mn-O bond lengths make it difficult to draw firm conclusions about their temperature dependence. However, the Mn-O(2) distance in phase 1 (magnetic) of $Sr_2NdMn_2O_7$ clearly lengthens on cooling from room temperature to 1.7 K whereas the corresponding bond in phase 2 contracts. There is a concomitant shortening of the bond Mn-O(1) in phase 1, but no corresponding change in phase 2. This can be linked with the presence of a relatively high Sr concentration on site Sr/Nd(1) in phase 2, and also with the lack of long-range magnetic ordering; the increased concentration of the larger cation on this site prevents the compression of the perovskite blocks, which would involve a shortening of Mn-O(1), and thus prevents the exchange striction which stabilizes antiferromagnetism in phase 1. The resolution of our data does not allow us to detect any significant temperature dependence in the bond lengths of $Sr_{1.9}Nd_{1.1}Mn_2O_7$. We are presently characterizing a wide range of samples in the series $Sr_{2-x}Ln_{1+x}Mn_2O_7$ (Ln is any lanthanide) (Ref. 13) in an attempt to gain further insight into the cation ordering in these materials and the consequences for magnetotransport properties.

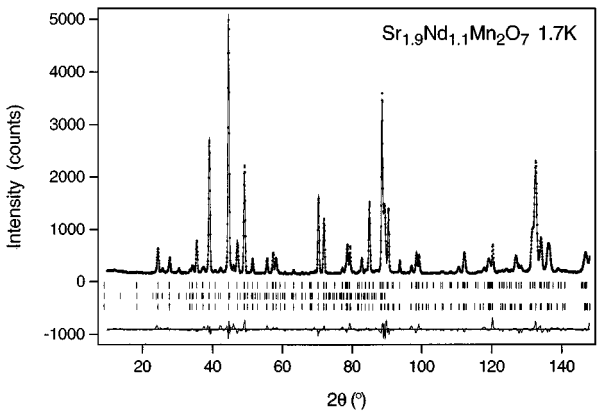

FIG. 12. Observed calculated and difference neutron powder diffraction patterns for $Sr_{1.9}Nd_{1.1}Mn_2O_7$ at 1.7 K ($\lambda \sim 1.6$ Å). Reflection positions are marked for the majority and minority phases as well as for the allowed magnetic reflections as in Fig. 4.

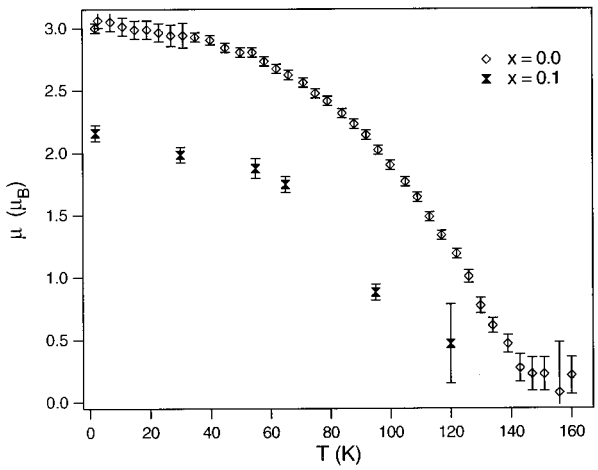

FIG. 13. The average ordered magnetic moment per Mn in $Sr_{2-x}Nd_{1+x}Mn_2O_7$ as a function of temperature.

It is interesting to compare the magnetic behavior described above with the magnetic susceptibility data presented previously.[9] The susceptibility of $Sr_2NdMn_2O_7$ shows a maximum at ~220 K. The results of our neutron scattering experiments show that this does not coincide with the onset of long range magnetic ordering, and the origin of this feature remains a matter for speculation. The local maximum in the susceptibility at ~140 K does however coincide with the appearance of magnetic Bragg scattering in the diffraction patterns and thus represents the magnetic ordering temperature. Hysteresis is apparent between the zero-field-cooled (zfc) and field-cooled (fc) susceptibilities below 140 K, and

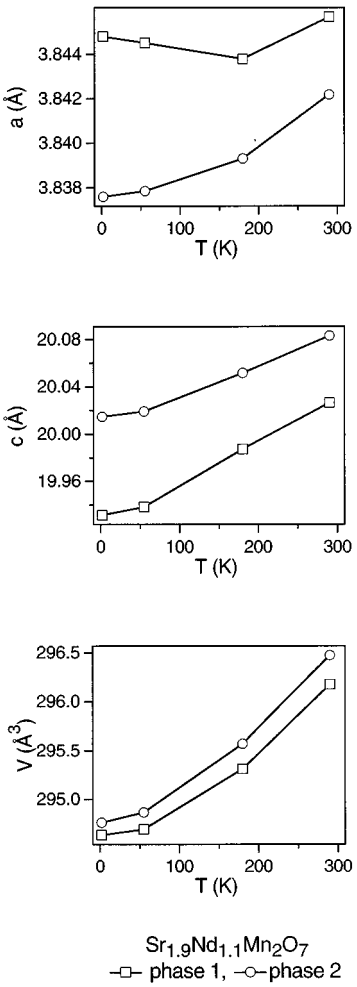

FIG. 14. Unit cell parameters a (a), c (b), and the cell volume (c) of $Sr_{1.9}Nd_{1.1}Mn_2O_7$ as a function of the temperature. Phase 2 is the majority phase.

this is compatible with the presence of two phases in our sample. We suggest that one of the phases (phase 1) is antiferromagnetic whereas the other (phase 2) is frustrated and shows no long-range order. This is of course consistent with our decision to include only one magnetic phase in the analysis of our neutron diffraction data. In the temperature range $30 \leqslant T/K \leqslant 140$ only the Mn cations are involved in the magnetic ordering, and it seems likely, in view of the absence of a strong Curie-like behavior in the susceptibility, that the magnetic moments of the Nd cations in the ordered phase are frozen in a spin-glass-like fashion and thus contribute to the observed hysteresis. The second local maximum in the susceptibility data, at ~30 K, is clearly associated with the onset of magnetic ordering of the Nd(2) cations within the rocksalt layers. The single ion anisotropy derived from the orbital contribution to the magnetic moment of Nd^{3+} presumably selects the z axis as the direction of spin alignment, and the anisotropy of the Mn sublattice is sufficiently weak for the magnetic moments of those cations to rotate some way towards the parallel alignment with Nd which is favored by exchange interactions. The Nd(1) cations at the center of the octahedral double layer have equal numbers of neighbors with spins aligned in two antiparallel directions. They are therefore frustrated and we believe they continue to form a spin-glass layer between the magnetized blocks. This is consistent with a representation analysis of the structure in that the spins of the Nd(1) cations have the wrong symmetry ($E_g^{xy}+A_{2g}^{z}$) to couple to the observed representations of the Mn sublattice ($E_u^{xy}+A_{1u}^{z}$). The z components of the Mn moments order with the same representation (A_{1u}^{z}) as the rocksalt layer Nd(2) moments, which only have a z component. There is no evidence in either the neutron data or the susceptibility data for a ferromagnetic component in this sample. The saturation value of the ordered magnetic moment of the Nd cations [$2.0(1)\mu_B$] lies between that ($1.1\mu_B$) found previously in Nd_2CuO_4 (Ref. 21) and the free ion value ($3.27\mu_B$). The differences presumably stem from a combination of crystal field effects, variations in the magnetic form factor used in data analysis, and the error in our phase fraction. The average oxidation state of the Mn cations in this compound is 3.5, and the ideal spin-only magnetic moment would thus be $3.5\mu_B$ if the localized electron model was applicable; it is not clear that this assumption is entirely valid in a compound which shows such unusual transport behavior. Furthermore, the measured moment is expected to be reduced below the theoretical value by the effects of covalency, and we therefore believe that the refined value of $3.08(4)\mu_B$ is not incompatible with our model. (The somewhat arbitrary choice of a form factor introduces some uncertainty into this parameter.)

The properties of $Sr_{1.9}Nd_{1.1}Mn_2O_7$ are similar to those of $Sr_2NdMn_2O_7$, but, as in the pseudocubic manganate perovskites, the differences between them are large considering how small a change (from 3.5 to 3.45) has occurred in the oxidation state of Mn. The relative phase fractions have changed markedly, the magnetic phase with the shorter a axis being the minority phase in $Sr_{1.9}Nd_{1.1}Mn_2O_7$. This might be a kinetic consequence of the sample preparation rather than a thermodynamic change, and more experimental work is needed to elucidate this point. (It should also be remembered that the phase fractions were particularly sensitive to the parameter set used in the Rietveld analysis.) The general features of the magnetic structures do not change, but the magnetic anisotropy is modified by the slightly enhanced concentration of Nd cations such that the Mn moments align along the z axis ($\phi=0$) in the low temperature phase. The average ordered magnetic moments of the Mn and Nd cations in the magnetic phase are significantly reduced compared with those in $Sr_2NdMn_2O_7$, suggesting that there is a considerable degree of magnetic frustration in both of the phases present in the Nd-rich sample. This conclusion is consistent with the magnetic susceptibility data on $Sr_{1.9}Nd_{1.1}Mn_2O_7$, which show hysteresis over a wide temperature range ($4 \leqslant T/K \leqslant 100$) but which, unlike those on $Sr_2NdMn_2O_7$, do not show well-defined transition temperatures.[9] The magnetoresistance of $Sr_{1.9}Nd_{1.1}Mn_2O_7$ is considerably greater than that of $Sr_2NdMn_2O_7$. It is therefore not surprising that differences in their magnetic properties are revealed by susceptibility and neutron diffraction experiments. It is, however, difficult to link the three sets of observations and to identify the structural features, either chemical or magnetic, which are important in the control of the magnetoresistance. If we initially assume that the CMR is associated with the magnetically ordered phase in each sample,

then the model we are searching for must account for a colossal magnetoresistance over a temperature range ($4 \leqslant T/K \leqslant 100$) which spans two distinct magnetic phases, both antiferromagnetic, in compounds which are insulators in the absence of an applied field. If this assumption is incorrect, and the CMR is associated with that part of the sample which does not show long-range magnetic order at any temperature, then we would have to rely on a model involving field-dependent spin alignment in a spin glass phase to account for our data over the whole temperature range. Such a model is defensible because it can be argued that CMR has previously only been observed in compounds having a spontaneous magnetization, and that phase 2 is more compatible with ferromagnetism by virtue of having the longer Mn-O(1) distance; that is the competing antiferromagnetic interactions are not stabilized by the crystal structure. However, the absence of CMR in other spin-glass manganates, for example the $n=1$ phase $La_{1-x}Sr_{1+x}MnO_4$ (Ref. 22) encourages us to rely on our original assumption. We can then suggest two mechanisms for CMR in the magnetically ordered phase 1 which merit further investigation. In the first we build a link with ferromagnetic CMR materials by considering the four-layer [Mn+Nd+Nd+Mn] blocks referred to above. These blocks carry a spontaneous magnetization for $T<30$ K in both $Sr_2NdMn_2O_7$ and $Sr_{1.9}Nd_{1.1}Mn_2O_7$. However, the ordered component of the cation magnetic moment is much reduced in the latter compared to the former. This suggests that a considerable amount of spin disorder is present on both the Nd and Mn sublattices in $Sr_{1.9}Nd_{1.1}Mn_2O_7$, even at 4 K. It is possible that the application of an external field reduces the spin disorder and hence the spin scattering of the Mn *d* electrons, thus reducing the resistivity in the *ab* plane of the crystal structure. This model would lead to a strongly two-dimensional conductivity. The persistence of the field dependence in the temperature region $30<T/K<120$, where the Nd layers within the blocks appear to be showing spin glass behavior, can be explained by a similar argument, that is that a strong external field causes an alignment of the Nd spins and a rotation of the Mn moments so that they are collinear with those of the rare earth cations. The model described above is consistent with the magnetoresistance of $Sr_2NdMn_2O_7$ being less than that of $Sr_{1.9}Nd_{1.1}Mn_2O_7$ because the atomic moments are more fully aligned in the latter in the absence of a magnetic field, and the application of a field can therefore have less influence. The principal difference between this model and that which assumes that the CMR occurs in phase 2 is that the former involves the interaction of ordered spins and glassy spins, rather than just relying on a glassy phase.

The second mechanism which we wish to propose is perhaps more intuitive because it focuses on the double octahedral layers which make up the perovskite blocks in the $n=2$ RP structure; there is thus a direct structural link with other known CMR materials. If the external field modifies the magnetic structure such that the magnetic moments of the Mn cations within a double layer became parallel, then the structure can still remain antiferromagnetic if neighboring double layers adopt opposite spin directions, as represented in Fig. 15. The symmetry representation of the Mn sublattice is thus changed to $E_g^{xy}+A_{2g}^{z}$, allowing this sublattice to couple to the Nd(1) cations in the center of the double layer. It has previously been shown that single perovskite layers in $n=1$ K_2NiF_4-like manganates do not show CMR, but the double ferromagnetic layers in the structure proposed may be thick enough to permit an effect. We are therefore suggesting that an effect previously seen in the bulk of a perovskite is occurring within a double layer.

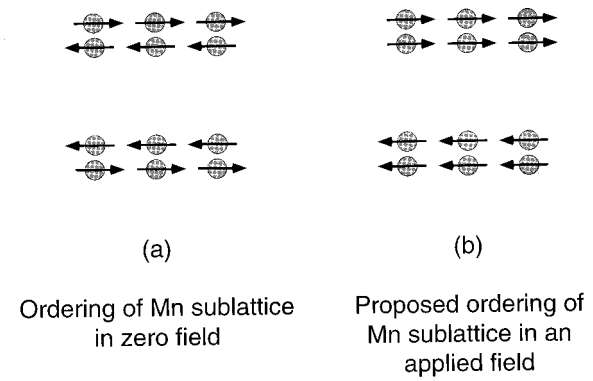

FIG. 15. Proposed change in magnetic structure of $Sr_{2-x}Nd_{1+x}Mn_2O_7$ in an applied magnetic field.

The appearance of our magnetization data[9] shows that any ferromagnetism in these samples remains a local rather than a bulk effect for fields of $\leqslant 5$ T. Both of the ''phase 1'' models described above provide a source of local ferromagnetism, and hence reduced electron scattering, by identifying magnetized blocks within the structure; they differ in where they place the interblock boundaries. Both of the models would lead to significant, albeit different, changes in the neutron diffraction pattern of $Sr_{2-x}Nd_{1+x}Mn_2O_7$ as a function of applied field, and we plan to carry out the appropriate measurements to distinguish between them in the near future. They are clearly both attempts to rationalize the data in a way that differs as little as possible from the currently accepted mechanism of CMR, which is based on double exchange in ferromagnets. It may be that, in the absence of true ferromagnetism, we should be more radical and seek a completely different explanation.

ACKNOWLEDGMENTS

We are grateful to the EPSRC and the Donors of the Petroleum Research Fund, administered by the American Chemical Society, for financial support and to D. E. Cox for useful discussions.

*Authors to whom correspondence should be addressed.

[1] A. Urushibara, Y. Moritomo, T. Arima, A. Asamitsu, G. Kido, and Y. Tokura, Phys. Rev. B **51**, 14 103 (1995).

[2] R. M. Kusters, J. Singleton, D. A. Keen, R. McGreevy, and W. Hayes, Physica B **155**, 362 (1989).

[3] Z. Zuotao and R. Yufang, J. Solid State Chem. **121**, 138 (1996).

[4] A. Maignan, C. Simon, V. Caignaert, and B. Raveau, J. Magn. Magn. Mater. **152**, L5 (1996).

[5] R. von Helmolt, J. Wecker, T. Lorenz, and K. Samwer, Appl. Phys. Lett. **67**, 14 (1995).

[6] Y. Shimakawa, Y. Kubo, and T. Manako, Nature **379**, 53 (1996).
[7] Y. Moritomo, A. Asamitsu, H. Kuwahara, and Y. Tokura, Nature **380**, 141 (1996).
[8] P. D. Battle, M. A. Green, N. S. Laskey, J. E. Millburn, M. J. Rosseinsky, S. P. Sullivan, and J. F. Vente, Chem. Commun. 767 (1996).
[9] P. D. Battle, S. J. Blundell, M. A. Green, W. Hayes, M. Honold, A. K. Klehe, N. S. Laskey, J. E. Millburn, L. Murphy, M. J. Rosseinsky, N. A. Samarin, J. Singleton, N. E. Sluchanko, S. P. Sullivan, and J. F. Vente, J. Phys. Condens. Matter **8**, L427 (1996).
[10] R. A. Mohan-Ram, P. Ganguly, and C. N. R. Rao, J. Solid State Chem. **70**, 82 (1987).
[11] M. Lamire and A. Daoudi, J. Solid State Chem. **55**, 327 (1984).
[12] S. N. Ruddlesden and P. Popper, Acta Crystallogr. **11**, 541 (1958).
[13] P. D. Battle, M. A. Green, N. S. Laskey, J. E. Millburn, M. J. Rosseinsky, S. P. Sullivan, and J. F. Vente, Chem. Mater. (to be published).
[14] J. Pannetier, Chem. Scr. **26A**, 131 (1986).
[15] A. W. Hewat, Mater. Sci. Forum **9**, 69 (1986).
[16] H. M. Rietveld, J. Appl. Crystallogr. **2**, 65 (1969).
[17] A. C. Larson and R. B. von Dreele (unpublished).
[18] R. E. Watson and A. J. Freeman, Acta Crystallogr. **14**, 27 (1961).
[19] M. Blume, A. J. Freeman, and R. E. Watson, J. Chem. Phys. **37**, 1245 (1962).
[20] S. Greenwald and J. S. Smart, Nature **166**, 523 (1950).
[21] M. J. Rosseinsky, K. Prassides, and P. Day, Chem. Commun. 1734 (1989).
[22] Y. Moritomo, Y. Tomioka, A. Asamitsu, and Y. Tokura, Phys. Rev. B **51**, 3297 (1995).